The Bazar Ophiolite of NW Iberia: a relic of the Iapetus–Tornquist Ocean in the Variscan suture

Sonia S. Martínez,[1] Axel Gerdes,[2] Ricardo Arenas[1] and Jacobo Abati[1]

[1]*Departamento de Petrología y Geoquímica e Instituto de Geociencias (CSIC), Universidad Complutense, 28040 Madrid, Spain;* [2]*Institut für Geowissenschaften, Goethe Universität, D-6438 Frankfurt am Main, Germany*

ABSTRACT

The Bazar Ophiolite, one of the ophiolitic units involved in the Variscan suture of NW Iberia, is mainly formed by metagabbroic high T amphibolites with N-MORB affinity. The ophiolite appears accreted under an arc-derived upper terrane affected by intermediate-P granulite facies metamorphism dated at 496–484 Ma. U-Th-Pb geochronology and Lu-Yb-Hf isotope geochemistry of zircons allow recognizing two growth stages. The first occurred during crystallization of the gabbroic protolith and has been dated at 495 ± 2 Ma, whereas the second one, interpreted as dating the high T metamorphism, yielded an age of 475 ± 2 Ma. The chronology of the Bazar Ophiolite and its accretionary history suggest that this unit is a relic of the Cambrian ocean located to the North of Gondwana, the Iapetus–Tornquist Ocean, accreted to a dissected arc during or before the early stages in the opening of the Rheic Ocean.

Introduction

The Variscan Belt of NW Iberia shows an impressive section of the suture zone of this orogen, developed in Carboniferous times by the collision of Gondwana and Laurussia during the final event of the Pangea assembly (Matte, 2001; Martínez Catalán *et al.*, 2009). The suture zone appears transported in several allochthonous complexes of which the Órdenes Complex has the largest size and includes the most varied group of exotic terranes (Fig. 1a). An arc-derived terrane generated in Cambrian times in the periphery of Gondwana appears in the uppermost position of the allochthonous pile (upper units of NW Iberia). During a subsequent event, this arc rifted from the main continent, drifted to the North and was finally accreted to the southern margin of Laurussia (Gómez Barreiro *et al.*, 2007; Díaz García *et al.*, 2010; Fuenlabrada *et al.*, 2010). A first metamorphic event affecting the arc terrane, with intermediate-P features and dated in the range 496–482 Ma, is considered related to the internal dynamics of the peri-Gondwanan arc (Abati *et al.*, 1999, 2007), whereas a second high-P and high-T event dated at c. 400–390 Ma developed during the collision with Laurussia (Ordoñez Casado *et al.*, 2001; Fernández-Suárez *et al.*, 2007). The arc-derived terrane is thrust over a group of different ophiolitic units (Fig. 1a). The ophiolites in turn thrust a lower terrane with high-P and intermediate-T metamorphism dated at c. 370 Ma (basal units of NW Iberia; Fig. 1a), interpreted as the edge of the Gondwanan margin subducted under Laurussia during the first stages of the collision, uplifted and incorporated to the allochthonous pile later on (Arenas *et al.*, 1995; Martínez Catalán *et al.*, 1996; Abati *et al.*, 2010).

The ophiolites outlining the Variscan suture were in general formed inside the Rheic Ocean domain, but they have typical compositions of island–arc tholeiites (Sánchez Martínez, 2009). Some of them, as the Vila de Cruces Ophiolite (Fig. 1a; Arenas *et al.*, 2007), were generated in the first stages of the opening of this ocean during Middle Cambrian times, due to the spreading of a back-arc basin. However, the most common ophiolites along the European Variscan Belt have shown ages at around c. 395 Ma, and their generation seems to be connected to the activity of an intra-Rheic subduction zone responsible for the main contractional event in this ocean. The Careón Ophiolite is the most representative supra–subduction zone ophiolite in NW Iberia (Fig. 1a; Díaz García *et al.*, 1999; Sánchez Martínez *et al.*, 2007). Nevertheless, there is an ophiolitic unit in the NW of the Iberian Massif, the Bazar Ophiolite (Fig. 1a), which shows lithological constitution and tectonothermal evolution distinctive and different from those shown by the other ophiolitic units. This article presents new U-Pb-Hf and Lu-Yb-Hf zircon data from the metagabbroic amphibolites of the Bazar Ophiolite. These new data, together with the chemical composition of the metagabbroic rocks and their metamorphic evolution, are not compatible with the generation of this ophiolite within the context of the Rheic Ocean, but they better suggest an origin related to a different older oceanic realm.

Correspondence: Sonia S. Martínez, Dpto. Petrología y Geoquímica, Universidad Complutense de Madrid. Jose Antonio Nováis 2, 28040, Madrid, Spain. Tel.: +34 618544373; e-mail: s.sanchez@geo.ucm.es

The Bazar Ophiolite

The Bazar Ophiolite is located in the westernmost part of the Ordenes Complex (Fig. 1a). It consists of an imbricate of tectonic slices, mainly constituted by metagabbroic rocks and a minor proportion of ultramafic rocks at the base of the unit (Díaz García, 1990). The main tectonic slice (Carballo – Bazar) is c. 4000 m thick and is composed of amphibolites and foliated metagabbros with high T foliation, which evolved from an initial granulite-facies tectonothermal event.

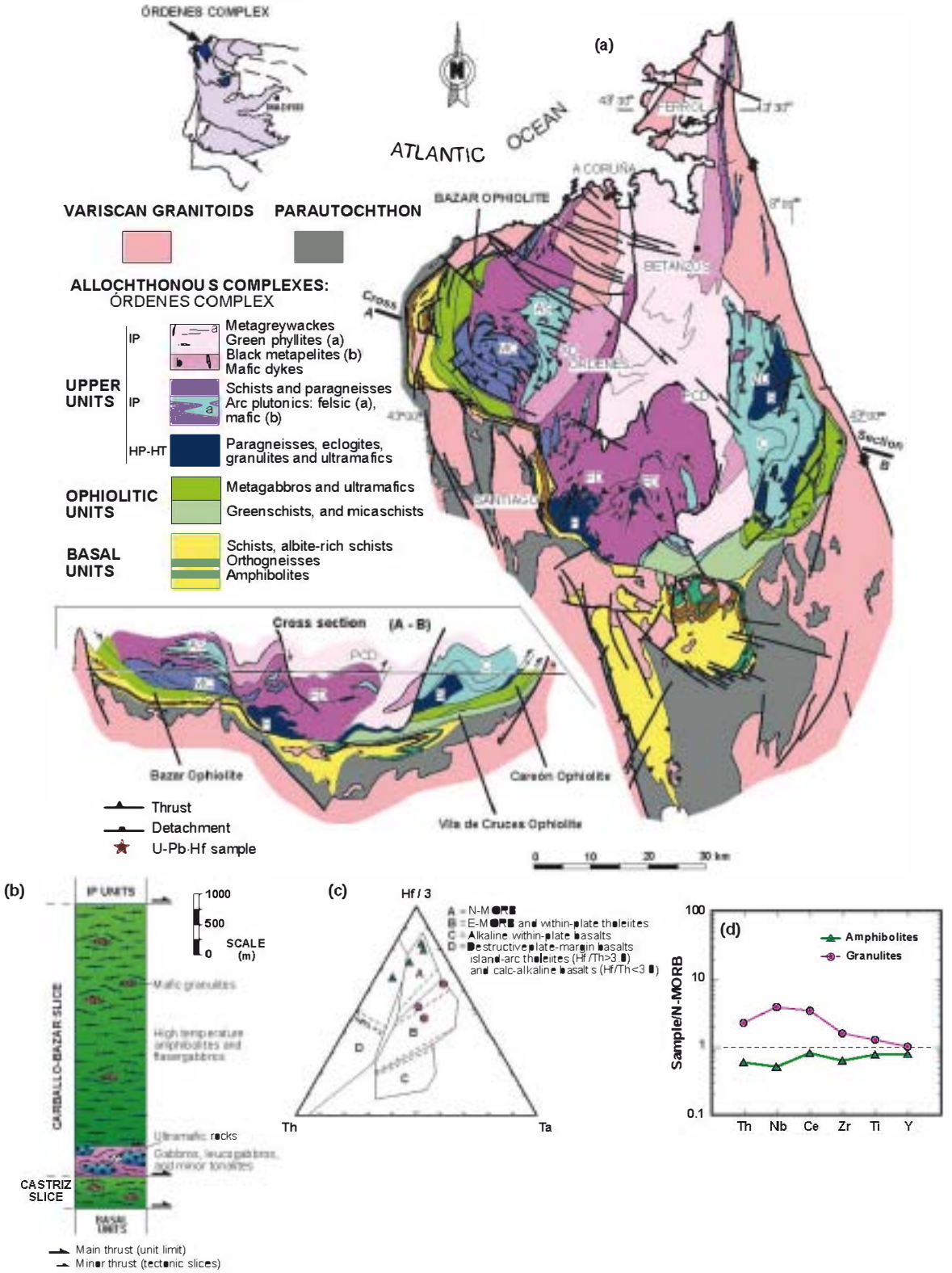

Fig. 1 (a) Geological map and cross-section of the Órdenes Complex with location of the Bazar Ophiolite and other ophiolitic units involved in the Variscan suture. (b) Representative section of the Bazar Ophiolite. (c) Th-Hf-Ta diagram (Wood, 1980) with projection of the metagabbroic amphibolites representing the most common lithology in the ophiolite, and the mafic granulites constituting uncommon minor bodies within the unit. (d) Normal-mid-ocean-ridge basalts (N-MORB) normalized trace-element patterns (average composition); selected elements and normalized values after Pearce (1996).

Scarce metric-sized boudins of mafic granoblastic granulites appear preserved within the metagabbros (Fig. 1b). These boudins appear wrapped by the high T foliation and their mineral associations indicate low-to-intermediate pressure conditions (plagioclase + clinopyroxene + orthopiroxene + hornblende + ilmenite ± garnet ± olivine). The lower section of the main slice has a different lithological composition, as mentioned before, which consists of relatively well-preserved gabbros and ultramafic rocks, with minor leucogabbros and tonalites (Fig. 1b). The granulite facies event is not recorded in this lower slice, which only shows an amphibolite facies metamorphism.

The geochemical features of the most representative lithologies of the Bazar Ophiolite appeared to be quite complex (Sánchez Martínez, 2009). Regarding the common amphibolites, which represent the most abundant lithological type, they show compositions equivalent to N-MORB (normal-mid-ocean ridge basalt, Fig. 1c, d) pointing to a tectonic setting possibly related to a divergent plate margin. There seems to be no evidence indicating some influence of a subduction zone in the generation of these gabbros unlike what has been registered in the other ophiolitic units described in NW Iberia (Sánchez Martínez *et al.*, 2009). However, the mafic granulites are transitional between MOR (mid-ocean ridge) and WP (within-plate) basalts with normalized trace element patterns similar to those of T-MORB generated in plume ridge interactions (Pearce, 1996).

Results of U-Th-Pb and Lu-Yb-Hf isotope analyses

From the amphibolite sample GCH-04-3, located at the top of the main tectonic slice (Fig. 1a), 71 zircon grains were analysed by U-Th-Pb LA-ICP-MS at the Goethe University Frankfurt (GUF), obtaining a set of 99 data (Fig. 2b; Table 1). Furthermore, 77 Hf isotope analyses were obtained in the same grains and crystal domains where the U-Th-Pb analyses were performed (Fig. 2d–f; Table 2). The analytical techniques applied for U-Th-Pb and Lu-Yb-Hf isotope determination are described in detail by Gerdes and Zeh (2006, 2009). The studied sample is one of the most representative metabasites of nematoblastic type of this mafic unit constituted by hornblende + plagioclase + clinozoisite + ilmenite + titanite + quartz. The zircon grains were subrounded and may reflect resorption of originally irregular and fragmented zircons, which are typical of mafic rocks. (Corfu *et al.*, 2003). These resorption processes frequently occur in zircons of high-grade metamorphic rocks (Hoskin and Black, 2000). Their size ranges between 100 and 300 μm and cathodoluminescence (CL) images were taken from all of them prior to their analysis to observe their internal structure. They show a combination of sector and fine oscillatory zoning, features that can be considered of igneous origin, and many of them also display irregular overgrowths or recrystallized domains lacking internal structure, which would be developed during the granulite-facies metamorphic event undergone by the ophiolitic unit (Fig. 2a).

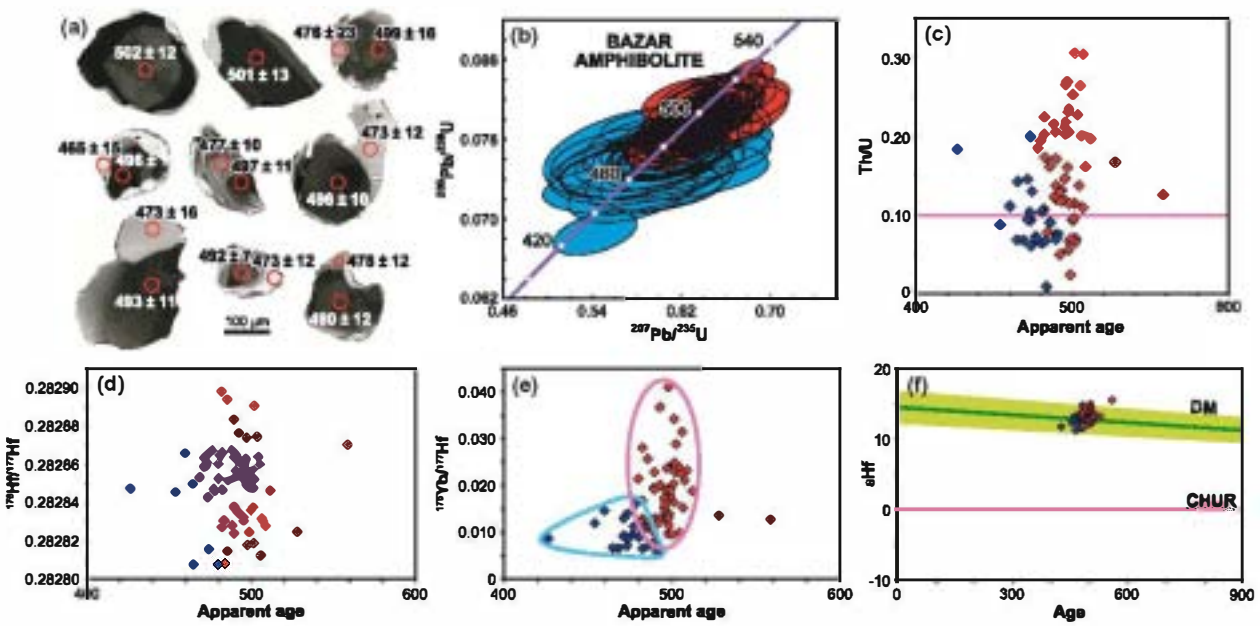

Fig. 2 (a) Cathodo-luminescence images of selected zircons of the Bazar amphibolite GCH-04-3, circles representing the spot size of U-Th-Pb analyses. (b) Concordia diagram showing the results of the U-Pb analyses, with two statistically coherent groups of data. (c) Th/U ratio versus apparent age diagram. (d) Initial $^{176}Hf/^{177}Hf$ versus apparent age diagram. (e) $^{176}Yb/^{177}Hf$ versus apparent age diagram, the different trends of each group of analyses appearing encircled. (f) εHf versus apparent age plot; the depleted mantle array (DM) is extrapolated from average modern-day values of mid-ocean ridge basalts (Chauvel and Blichert-Toft, 2001), assuming a linear behaviour from εHf = 2 at 4000 Ma (Vervoort and Blichert-Toft, 1999). In all diagrams, red symbols = zircon cores; blue symbols = zircon overgrowths recrystallized domains.

Table 1 Results of U-Th-Pb LA-ICP-MS analyses of zircon from the sample of Bazar amphibolite.

Grain	L-No.	$^{207}Pb^*$ (cps)	U† (ppm)	Pb† (ppm)	Th/† U	$^{206}Pb/^{204}Pb$	$^{206}Pb/‡ ^{238}U$	±2σ/ (%)	$^{207}Pb/‡ ^{235}U$	±2σ/ (%)	$^{207}Pb/‡ ^{206}Pb$	±2σ/ (%)	Rho§	Age (Ma) $^{206}Pb/^{238}U$	±2σ	$^{207}Pb/^{235}U$	±2σ	$^{207}Pb/‡ ^{206}Pb$	±2σ	Conc¶ (%)
1B	a-3	2494	71	5	0.12	8679	0.07886	2.4	0.6258	4.1	0.05756	3.3	0.59	489	11	493	16	513	73	95
2A	a-5	785	25	2	0.06	1581	0.07644	2.8	0.6107	6.3	0.05794	5.6	0.44	475	13	484	25	528	124	90
2B	a-6	4675	137	11	0.27	10449	0.07999	2.0	0.6352	3.0	0.05759	2.2	0.67	496	10	499	12	514	49	96
2B	a-7	471	15	1	0.09	1667	0.07618	2.6	0.5933	7.5	0.05649	7.0	0.35	473	12	473	29	472	155	100
3	a-10	433	13	1	0.09	1520	0.07826	2.5	0.6145	6.8	0.05695	6.3	0.37	486	12	486	27	490	139	99
3	a-11	390	12	1	0.09	1402	0.07457	2.9	0.5726	8.9	0.05569	8.4	0.33	464	13	460	33	440	187	105
4	a-12	1498	50	4	0.12	5283	0.07873	2.2	0.6137	4.8	0.05654	4.2	0.47	489	11	486	19	473	94	103
5	a-14	1974	62	5	0.13	6919	0.07912	2.8	0.6210	4.0	0.05692	2.9	0.69	491	13	490	16	489	65	100
7	a-18	1707	52	4	0.08	1557	0.07889	2.5	0.6204	3.8	0.05704	2.9	0.66	490	12	490	15	493	64	99
7	a-19	332	26	2	0.17	580	0.07692	2.6	0.6054	8.0	0.05709	7.5	0.33	478	12	481	31	495	165	96
8	a-22	953	36	2	0.18	3325	0.06839	2.6	0.5412	5.8	0.05739	5.1	0.45	426	11	439	21	507	113	84
11	a-26	3140	117	9	0.02	2239	0.08043	2.0	0.6281	3.3	0.05663	2.6	0.62	499	10	495	13	477	57	104
12	a-27	1662	64	5	0.20	2646	0.07770	2.2	0.6124	4.6	0.05717	4.0	0.49	482	10	485	18	498	88	97
13	a-28	4546	171	13	0.08	1758	0.07795	2.1	0.6254	3.2	0.05819	2.4	0.65	484	10	493	13	537	53	90
15	a-32	3923	151	12	0.22	13642	0.07997	2.4	0.6319	3.3	0.05731	2.2	0.73	496	12	497	13	503	49	99
16	a-33	3670	140	11	0.12	12700	0.07986	2.8	0.6341	4.0	0.05759	2.9	0.70	495	13	499	16	514	63	96
16	a-34	1082	44	3	0.06	460	0.07622	2.7	0.6000	5.6	0.05709	4.9	0.48	474	12	477	21	495	108	96
21	a-42	4005	156	12	0.16	13916	0.07819	2.5	0.6194	3.4	0.05745	2.2	0.75	485	12	489	13	509	49	95
21	a-43	1450	47	4	0.19	568	0.07697	3.0	0.6218	6.5	0.05859	5.7	0.47	478	14	491	26	552	125	87
23	a-44	2599	98	8	0.22	970	0.07767	3.0	0.6222	4.5	0.05810	3.3	0.67	482	14	491	18	533	73	90
24	a-45	2773	112	9	0.14	9506	0.07889	2.1	0.6310	3.6	0.05801	3.0	0.57	489	10	497	14	530	65	92
24	a-46	532	27	2	0.13	264	0.07544	3.1	0.6001	10.4	0.05769	9.9	0.30	469	14	477	40	518	217	90
25	a-47	3079	112	10	0.30	4281	0.08187	2.4	0.6290	5.8	0.05572	5.3	0.41	507	12	495	23	441	118	115
30	a-55	3383	136	11	0.13	3200	0.08298	3.1	0.6640	3.7	0.05804	2.1	0.82	514	15	517	15	531	47	97
34	b-6	2910	119	9	0.13	2746	0.07944	2.6	0.6203	4.0	0.05664	3.0	0.65	493	12	490	15	477	67	103
34	b-7	1251	49	4	0.16	4333	0.07686	3.0	0.6158	5.3	0.05811	4.4	0.56	477	14	487	21	534	96	89
35	b-8	1389	65	5	0.11	4804	0.07760	2.2	0.6228	4.3	0.05821	3.7	0.51	482	10	492	17	538	80	90
35	b-9	435	18	1	0.11	1476	0.07393	3.6	0.6012	9.2	0.05898	8.4	0.39	460	16	478	36	566	184	81
35	b-10	382	17	1	0.11	596	0.07270	3.6	0.5756	8.3	0.05742	7.5	0.43	452	16	462	31	508	164	89
39	b-19	2353	108	8	0.19	1020	0.07728	2.1	0.6090	3.5	0.05715	2.8	0.60	480	10	483	14	497	62	96
41A	b-22	3841	169	13	0.17	13509	0.07771	2.2	0.6149	3.3	0.05740	2.4	0.67	482	10	487	13	507	54	95
41A	b-23	362	16	1	0.11	1260	0.07743	3.6	0.6170	7.8	0.05779	6.9	0.46	481	17	488	31	522	152	92
42	b-25	1347	60	5	0.17	4678	0.07889	2.0	0.6262	4.6	0.05757	4.1	0.44	489	10	494	18	514	90	95
42	b-26	350	16	1	0.09	288	0.07584	3.2	0.6031	7.4	0.05768	6.6	0.43	471	14	479	29	517	146	91
42	b-27	205	9	1	0.09	728	0.07297	2.9	0.5759	11.6	0.05724	11.2	0.25	454	13	462	44	501	247	91
43	b-28	3588	151	12	0.15	12352	0.07984	2.7	0.6449	3.5	0.05858	2.3	0.75	495	13	505	14	552	51	90
45	b-32	2008	91	7	0.16	3412	0.08212	2.3	0.6399	4.0	0.05651	3.3	0.57	509	11	502	16	473	73	108
46	b-33	4652	196	17	0.21	4146	0.08309	2.5	0.6751	3.5	0.05893	2.5	0.71	515	12	524	15	564	54	91
47	b-34	1876	85	7	0.12	1120	0.07941	2.3	0.6293	4.1	0.05747	3.5	0.54	493	11	496	16	510	76	97
47	b-35	282	14	1	0.10	1034	0.07605	3.5	0.5799	11.0	0.05530	10.4	0.32	473	16	464	42	424	233	111
48	b-37	1651	71	5	0.07	5678	0.08098	2.4	0.6550	4.5	0.05866	3.8	0.53	502	12	512	18	554	84	91

Table 1 Continued.

Grain	L-No.	$^{207}Pb^*$ (cps)	U† (ppm)	Pb† (ppm)	Th/† U	$^{206}Pb/^{204}Pb$	$^{206}Pb/‡ ^{238}U$	±2σ/ (%)	$^{207}Pb/‡ ^{235}U$	±2σ/ (%)	$^{207}Pb/‡ ^{206}Pb$	±2σ/ (%)	Rho§	Age (Ma) $^{206}Pb/^{238}U$	±2σ	$^{207}Pb/^{235}U$	±2σ	$^{207}Pb/‡ ^{206}Pb$	±2σ	Conc¶ (%)
49	b-38	775	35	3	0.25	2718	0.08077	3.5	0.6398	6.9	0.05745	5.9	0.51	501	17	502	28	509	130	98
50	b-39	665	29	2	0.20	491	0.08163	2.7	0.6655	6.5	0.05913	5.9	0.41	506	13	518	27	572	129	88
52	b-41	1845	76	6	0.06	448	0.08024	3.2	0.6706	5.6	0.06061	4.7	0.56	498	15	521	23	626	100	80
52	b-42	415	20	1	0.06	1504	0.07730	3.3	0.5970	8.9	0.05601	8.3	0.37	480	15	475	34	453	184	106
53	b-44	1283	61	5	0.11	4489	0.08086	2.6	0.6433	5.3	0.05770	4.7	0.49	501	13	504	21	518	103	97
54	b46	1243	54	4	0.23	782	0.08126	2.3	0.6585	4.6	0.05878	4.0	0.51	504	11	514	19	559	86	90
55	b48	1760	77	7	0.31	1325	0.08100	2.4	0.6384	4.3	0.05716	3.6	0.56	502	12	501	17	498	79	101
58	b51	1720	78	6	0.07	3086	0.08091	2.4	0.6470	4.1	0.05799	3.3	0.59	502	12	507	16	529	72	95
59	b53	2501	117	10	0.20	2938	0.08268	2.5	0.6619	4.2	0.05806	3.3	0.59	512	12	516	17	532	73	96
62	b54	1873	87	7	0.09	1068	0.08066	2.3	0.6375	4.4	0.05732	3.8	0.51	500	11	501	17	504	83	99
62	b55	337	18	1	0.08	1194	0.07910	2.3	0.6207	9.7	0.05691	9.5	0.23	491	11	490	39	488	209	101
63	c-1	4247	188	16	0.27	5955	0.08017	1.4	0.6448	3.2	0.05833	2.8	0.45	497	7	505	13	542	62	92
64	c-2	1672	74	6	0.24	5791	0.08034	1.6	0.6500	3.9	0.05868	3.5	0.41	498	8	508	16	555	77	90
64	c-3	780	36	3	0.01	2767	0.07786	3.1	0.6136	5.8	0.05716	5.0	0.52	483	14	486	23	498	109	97
66	c-4	3001	137	11	0.14	10476	0.08180	1.8	0.6556	3.4	0.05812	2.9	0.51	507	9	512	14	534	64	95
68	c-7	3701	171	14	0.23	1287	0.08025	1.5	0.6378	3.0	0.05764	2.7	0.49	498	7	501	12	516	58	96
70	c-8	2511	116	9	0.20	8707	0.07990	2.0	0.6410	3.8	0.05818	3.2	0.53	496	10	503	15	537	70	92
70	c-9	446	20	1	0.10	1506	0.07732	2.9	0.6438	7.4	0.06039	6.9	0.38	480	13	505	30	618	149	78
72	c-10	2819	137	11	0.21	9764	0.08026	1.5	0.6475	3.3	0.05851	2.9	0.45	498	7	507	13	549	64	91
74	c-12	3300	158	12	0.07	11539	0.08028	1.9	0.6426	3.5	0.05806	3.0	0.54	498	9	504	14	532	65	94
76	c-14	3389	177	14	0.10	11813	0.08083	1.5	0.6500	3.3	0.05832	2.9	0.46	501	7	508	13	542	64	92
76	c-15	330	17	1	0.07	1138	0.07888	2.9	0.6399	7.7	0.05883	7.1	0.38	489	14	502	31	561	155	87
83	c-20	375	22	2	0.12	458	0.07785	3.8	0.6279	7.3	0.05849	6.3	0.51	483	18	495	29	548	138	88
87	c-22	695	41	3	0.14	2469	0.08137	2.6	0.6430	5.7	0.05731	5.0	0.46	504	13	504	23	503	111	100
88	c-24	2171	127	11	0.26	7651	0.08155	3.3	0.6483	4.4	0.05766	2.9	0.75	505	16	507	18	517	64	98
91	c-26	2051	129	10	0.21	7269	0.07888	2.0	0.6220	4.2	0.05718	3.6	0.49	489	10	491	16	499	80	98
99	c-31	686	45	4	0.17	2405	0.08207	2.6	0.6521	6.7	0.05762	6.2	0.39	508	13	510	27	516	136	99
99	c-32	245	19	1	0.07	880	0.07539	3.7	0.5922	11.7	0.05697	11.1	0.32	469	17	472	45	490	245	96
100	c-33	2207	152	12	0.11	1126	0.08172	1.8	0.6510	3.7	0.05777	3.3	0.49	506	9	509	15	521	72	97
102	c-37	1962	146	12	0.21	1535	0.07995	2.4	0.6437	3.9	0.05840	3.1	0.60	496	11	505	16	545	69	91
102	c-38	201	15	1	0.14	732	0.07476	3.3	0.6041	12.9	0.05861	12.4	0.25	465	15	480	50	553	271	84
105	c-39	1613	127	10	0.11	5542	0.08029	1.9	0.6417	3.8	0.05797	3.3	0.49	498	9	503	15	528	73	94
106	c-40	453	42	3	0.15	1640	0.07582	2.0	0.5845	7.5	0.05591	7.2	0.27	471	9	467	28	449	161	105
115	c-45	723	66	5	0.07	2549	0.08044	3.4	0.6353	6.7	0.05728	5.8	0.51	499	16	499	27	502	127	99
115	c-46	124	12	1	0.07	462	0.07667	5.0	0.5832	12.4	0.05517	11.4	0.40	476	23	467	47	419	254	114
116A	c-47	4282	385	31	0.16	14973	0.08009	2.4	0.6410	3.3	0.05804	2.3	0.72	497	11	503	13	531	50	93
116A	c-48	1001	102	7	0.07	3642	0.07684	2.3	0.5913	5.0	0.05581	4.5	0.45	477	10	472	19	445	99	107
116B	c-49	1715	178	13	0.05	6241	0.07932	1.4	0.6117	4.0	0.05593	3.7	0.36	492	7	485	15	449	82	109
116B	c-50	449	48	4	0.20	1585	0.07618	2.6	0.6049	7.2	0.05759	6.8	0.35	473	12	480	28	514	149	92
117	c-53	781	87	7	0.13	2769	0.07771	2.8	0.6106	6.0	0.05699	5.3	0.46	482	13	484	23	491	117	98
118A	c-54	2854	305	23	0.09	9986	0.07821	2.1	0.6218	3.7	0.05767	3.1	0.56	485	10	491	15	517	67	94

Table 1 Continued.

Grain	L-No.	$^{207}Pb^*$ (cps)	U† (ppm)	Pb† (ppm)	Th/† U	$^{206}Pb/^{204}Pb$	$^{206}Pb/‡ ^{238}U$	±2σ/ (%)	$^{207}Pb/‡ ^{235}U$	±2σ/ (%)	$^{207}Pb/‡ ^{206}Pb$	±2σ/ (%)	Rho§	Age (Ma) $^{206}Pb/^{238}U$	±2σ	$^{207}Pb/^{235}U$	±2σ	$^{207}Pb/‡ ^{206}Pb$	±2σ	Conc¶ (%)
118A	c-55	353	38	3	0.07	1222	0.07470	4.2	0.6052	8.0	0.05876	6.8	0.52	464	19	481	31	558	148	83
118B	d-1	2073	91	7	0.13	7190	0.07926	2.2	0.6182	4.1	0.05658	3.5	0.53	492	10	489	16	475	78	104
119	d-3	2971	132	11	0.23	10303	0.07843	2.0	0.6135	3.4	0.05672	2.8	0.59	487	9	486	13	481	61	101
119	d-4	545	23	2	0.13	1150	0.07632	2.8	0.6269	9.6	0.05957	9.2	0.29	474	13	494	38	588	200	81
121	d-5	717	31	2	0.07	1111	0.07770	2.8	0.6136	6.1	0.05728	5.4	0.45	482	13	486	24	502	119	96
121	d-6	5402	236	19	0.23	18769	0.08045	2.2	0.6290	2.9	0.05670	1.9	0.76	499	11	495	12	480	42	104
125	d-10	6127	267	21	0.13	21185	0.08107	2.2	0.6375	2.9	0.05703	1.8	0.77	503	11	501	11	493	40	102
125	d-11	3086	140	11	0.10	3387	0.07852	2.2	0.6108	3.7	0.05642	2.9	0.60	487	10	484	14	469	65	104
126A	d-12	3347	151	11	0.04	3519	0.07948	2.4	0.6373	3.8	0.05815	3.0	0.62	493	11	501	15	535	65	92
126B	d-14	2485	112	9	0.11	1513	0.07862	2.6	0.6337	4.1	0.05846	3.2	0.62	488	12	498	16	547	71	89
127	d-15	2694	118	9	0.17	9067	0.07865	2.4	0.6347	3.6	0.05853	2.7	0.66	488	11	499	14	550	58	89
128	d-17	3153	139	11	0.21	2549	0.07881	1.8	0.6334	3.1	0.05830	2.5	0.59	489	9	498	12	541	55	90
130	d-20	2823	130	10	0.22	1869	0.07869	2.0	0.6102	3.3	0.05624	2.5	0.63	488	10	484	13	462	56	106
134	d-25	2709	124	9	0.08	9236	0.07819	2.2	0.6239	4.0	0.05787	3.4	0.55	485	10	492	16	525	74	92
135	d-27	1977	91	7	0.23	6549	0.07992	2.2	0.6554	3.8	0.05948	3.1	0.59	496	11	512	15	585	67	85
135	d-28	183	9	1	0.09	646	0.07479	3.8	0.5834	11.6	0.05657	11.0	0.32	465	17	467	44	475	243	98
140	d-33	1765	82	6	0.09	5955	0.08232	2.5	0.6615	4.4	0.05827	3.7	0.56	510	12	516	18	540	80	94

Diameter of laser spot = 20 pm; depth of crater ca. 15 μm.

*Within run background-corrected mean ^{207}Pb signal in counts per second.

†U and Pb content and Th/U ratio were calculated relative to GJ-1 reference (LA-ICP-MS values).

‡Corrected for background, common Pb and within-run Pb/U fractionation and subsequently normalized to GJ-1 (ID-TIMS value/measured value). $^{207}Pb/^{235}U$ calculated using $^{207}Pb/^{206}Pb/(^{238}U/^{206}Pb \times 1/137.88)$. Uncertainties propagated following Gerdes and Zeh (2006, 2009).

§Rho is the error correlation of the $^{206}Pb/^{238}U$ and $^{207}Pb/^{235}U$ errors.

¶Percent concordance = $^{206}Pb/^{238}U$ age/$^{207}Pb/^{206}Pb$ age × 100.

Table 2 LA-MC-ICPMS Lu-Hf isotope data of zircon from the sample of Bazar amphibolite

L-No.	$^{176}Yb/^{177}Hf$*	±2σ	$^{176}Lu/^{177}Hf$*	±2σ	$^{178}Hf/^{177}Hf$	$^{180}Hf/^{177}Hf$	Sig_{Hf}† (V)	$^{176}Hf/^{177}Hf$	±2σ‡	$^{176}Hf/^{177}Hf_{(t)}$	εHf(t) §	±2σ	T_{DM2}¶ (Ga)	Age** (Ma)	±2σ
a-3	0.0194	16	0.00074	5	1.46717	1.88676	6	0.282845	29	0.282838	12.8	0.7	0.61	489	11
a-6	0.0130	11	0.00049	3	1.46715	1.88670	8	0.282865	27	0.282860	13.7	0.6	0.56	496	10
a-7	0.0071	6	0.00027	2	1.46720	1.88669	6	0.282864	24	0.282861	13.2	0.5	0.57	473	12
a-10	0.0070	6	0.00028	2	1.46717	1.88681	7	0.282854	29	0.282852	13.2	0.7	0.58	486	12
a-12	0.0125	11	0.00045	3	1.46715	1.88671	7	0.282832	26	0.282828	12.4	0.6	0.63	489	11
a-14	0.0126	11	0.00045	3	1.46716	1.88656	8	0.282861	23	0.282857	13.5	0.5	0.57	491	13
a-18	0.0080	7	0.00031	2	1.46715	1.88669	6	0.282855	29	0.282852	13.3	0.7	0.58	490	12
a-22	0.0086	8	0.00034	2	1.46707	1.88656	7	0.282850	26	0.282847	11.7	0.6	0.62	426	11
a-26	0.0178	14	0.00083	5	1.46719	1.88670	6	0.282859	30	0.282851	13.5	0.7	0.58	499	10
a-27	0.0129	11	0.00049	3	1.46721	1.88663	6	0.282869	26	0.282864	13.6	0.6	0.56	482	10
a-28	0.0114	13	0.00041	4	1.46724	1.88689	8	0.282812	28	0.282808	11.6	0.7	0.67	484	10
a-32	0.0142	11	0.00053	3	1.46717	1.88662	7	0.282857	25	0.282852	13.4	0.5	0.58	496	12
a-33	0.0151	12	0.00054	4	1.46722	1.88690	7	0.282836	24	0.282831	12.7	0.5	0.62	495	13
a-34	0.0087	7	0.00033	2	1.46727	1.88687	7	0.282846	24	0.282843	12.6	0.5	0.60	474	12
a-42	0.0112	9	0.00041	3	1.46722	1.88688	8	0.282818	23	0.282814	11.9	0.5	0.66	485	12
a-43	0.0161	13	0.00062	4	1.46717	1.88649	7	0.282852	32	0.282846	12.8	0.8	0.60	478	14
a-44	0.0168	14	0.00064	4	1.46716	1.88667	7	0.282833	24	0.282827	12.3	0.5	0.63	482	14
a-45	0.0129	11	0.00049	3	1.46713	1.88663	7	0.282828	27	0.282824	12.3	0.6	0.63	489	10
a-47	0.0211	17	0.00077	5	1.46712	1.88671	7	0.282838	29	0.282830	12.9	0.7	0.61	507	12
a-55	0.0128	10	0.00048	3	1.46707	1.88652	6	0.282875	25	0.282871	14.5	0.6	0.53	514	15
b-6	0.0367	32	0.00082	5	1.46727	1.88709	8	0.282863	34	0.282855	13.5	1.2	0.57	493	12
b-8	0.0121	12	0.00031	2	1.46728	1.88697	4	0.282901	41	0.282898	14.7	1.5	0.49	482	10
b-9	0.0146	12	0.00042	3	1.46727	1.88665	4	0.282870	52	0.282866	13.1	1.8	0.56	460	16
b-19	0.0214	17	0.00053	3	1.46723	1.88671	10	0.282865	26	0.282860	13.4	0.9	0.57	480	10
b-22	0.0281	23	0.00071	4	1.46713	1.88673	7	0.282873	31	0.282866	13.6	1.1	0.55	482	10
b-23	0.0095	8	0.00026	2	1.46723	1.88679	11	0.282867	32	0.282865	13.5	1.1	0.56	481	17
b-25	0.0228	20	0.00055	3	1.46721	1.88668	8	0.282858	26	0.282853	13.3	0.9	0.58	489	10
b-26	0.0129	13	0.00033	3	1.46725	1.88654	9	0.282866	32	0.282863	13.3	1.1	0.56	471	14
b-27	0.0120	11	0.00031	2	1.46721	1.88678	9	0.282848	29	0.282846	12.3	1.0	0.61	454	13
b-28	0.0172	14	0.00039	2	1.46720	1.88704	7	0.282836	29	0.282832	12.7	1.0	0.62	495	13
b-32	0.0232	19	0.00058	3	1.46720	1.88686	9	0.282833	23	0.282828	12.9	0.8	0.62	509	11
b-34	0.0201	16	0.00051	3	1.46719	1.88689	8	0.282881	40	0.282877	14.2	1.4	0.53	493	11
b-35	0.0090	8	0.00027	2	1.46726	1.88663	12	0.282861	23	0.282859	13.2	0.8	0.57	473	16
b-37	0.0228	19	0.00053	3	1.46724	1.88662	7	0.282895	29	0.282890	14.9	1.0	0.50	502	12
b-38	0.0204	18	0.00048	3	1.46722	1.88644	8	0.282862	30	0.282857	13.7	1.0	0.56	501	17
b-39	0.0315	25	0.00074	4	1.46722	1.88690	9	0.282819	28	0.282812	12.3	1.0	0.65	506	13
b-41	0.0097	9	0.00031	2	1.46722	1.88651	13	0.282877	21	0.282874	14.2	0.7	0.53	498	15
b-42	0.0090	7	0.00025	1	1.46720	1.88705	12	0.282810	26	0.282808	11.5	0.9	0.67	480	15
b-44	0.0342	28	0.00080	5	1.46719	1.88688	9	0.282855	24	0.282848	13.4	0.8	0.58	501	13
b-46	0.0241	20	0.00056	3	1.46721	1.88653	8	0.282880	24	0.282874	14.4	0.9	0.53	504	11
b-48	0.0289	23	0.00069	4	1.46719	1.88689	8	0.282859	34	0.282852	13.6	1.2	0.57	502	12
b-51	0.0248	20	0.00060	4	1.46722	1.88671	9	0.282825	31	0.282819	12.4	1.1	0.64	502	12
b-53	0.0188	15	0.00046	3	1.46723	1.88686	9	0.282851	30	0.282846	13.6	1.0	0.58	512	12
b-54	0.0095	8	0.00023	1	1.46724	1.88647	8	0.282838	31	0.282836	13.0	1.1	0.61	500	11

Table 2 Continued

L-No.	$^{176}Yb/^{177}Hf$*	±2σ	$^{176}Lu/^{177}Hf$*	±2σ	$^{178}Hf/^{177}Hf$	$^{180}Hf/^{177}Hf$	Sig_{Hf}† (V)	$^{176}Hf/^{177}Hf$	±2σ‡	$^{176}Hf/^{177}Hf_{(t)}$	εHf(t) §	±2σ	T_{DM2}¶ (Ga)	Age** (Ma)	±2σ
b-55	0.0059	5	0.00018	1	1.46725	1.88622	11	0.282866	30	0.282865	13.8	1.1	0.55	491	11
c-1	0.0238	19	0.00070	4	1.46725	1.88675	12	0.282855	22	0.282849	13.3	0.8	0.58	497	7
c-2	0.0139	11	0.00043	3	1.46723	1.88649	4	0.282856	36	0.282852	13.5	1.3	0.57	498	8
c-3	0.0109	9	0.00036	2	1.46719	1.88674	5	0.282834	37	0.282830	12.4	1.3	0.62	483	14
c-7	0.0190	16	0.00058	4	1.46723	1.88667	5	0.282854	27	0.282849	13.4	0.9	0.58	498	7
c-8	0.0161	13	0.00052	3	1.46721	1.88660	5	0.282864	27	0.282859	13.7	0.9	0.56	496	10
c-9	0.0089	8	0.00034	2	1.46724	1.88656	4	0.282856	43	0.282853	13.1	1.5	0.58	480	13
c-10	0.0131	11	0.00043	3	1.46726	1.88661	5	0.282860	39	0.282856	13.6	1.4	0.57	498	7
c-12	0.0411	33	0.00135	8	1.46723	1.88676	6	0.282867	32	0.282854	13.5	1.1	0.57	498	9
c-14	0.0164	14	0.00053	3	1.46720	1.88647	6	0.282842	25	0.282837	13.0	0.9	0.60	501	7
c-15	0.0074	6	0.00025	2	1.46723	1.88649	5	0.282866	28	0.282863	13.7	1.0	0.56	489	14
c-22	0.0099	8	0.00034	2	1.46722	1.88693	6	0.282867	32	0.282864	14.0	1.1	0.55	504	13
c-24	0.0226	18	0.00071	4	1.46721	1.88678	7	0.282867	30	0.282860	13.9	1.1	0.56	505	16
c-26	0.0191	15	0.00060	4	1.46727	1.88648	6	0.282889	29	0.282883	14.4	1.0	0.52	489	10
c-31	0.0137	15	0.00043	4	1.46722	1.88682	6	0.282829	34	0.282825	12.8	1.2	0.62	508	13
c-32	0.0066	5	0.00023	1	1.46725	1.88675	7	0.282855	26	0.282853	12.9	0.9	0.59	469	17
c-33	0.0153	13	0.00049	3	1.46723	1.88670	5	0.282836	35	0.282832	12.9	1.3	0.61	506	9
c-37	0.0190	17	0.00063	4	1.46721	1.88655	6	0.282859	31	0.282853	13.5	1.1	0.58	496	11
c-38	0.0067	6	0.00022	1	1.46726	1.88681	6	0.282810	29	0.282808	11.2	1.0	0.68	465	15
c-39	0.0115	9	0.00038	2	1.46730	1.88687	7	0.282821	30	0.282818	12.3	1.1	0.64	498	9
c-40	0.0092	8	0.00032	2	1.46727	1.88662	6	0.282862	31	0.282859	13.1	1.1	0.57	471	9
c-45	0.0190	15	0.00059	4	1.46727	1.88680	10	0.282830	26	0.282824	12.5	0.9	0.63	499	16
c-46	0.0095	9	0.00033	3	1.46721	1.88658	5	0.282870	30	0.282867	13.5	1.1	0.55	476	23
c-47	0.0236	22	0.00073	5	1.46725	1.88640	6	0.282870	30	0.282863	13.8	1.1	0.55	497	11
c-48	0.0112	9	0.00037	2	1.46719	1.88679	6	0.282850	29	0.282847	12.8	1.0	0.59	477	10
c-49	0.0128	13	0.00048	4	1.46728	1.88679	6	0.282866	35	0.282862	13.7	1.2	0.56	492	7
c-50	0.0140	11	0.00052	3	1.46727	1.88653	5	0.282869	34	0.282865	13.4	1.2	0.56	473	12
c-54	0.0258	22	0.00079	5	1.46720	1.88637	6	0.282901	33	0.282894	14.7	1.2	0.50	485	10
c-55	0.0067	6	0.00025	2	1.46722	1.88670	5	0.282852	34	0.282850	12.6	1.2	0.59	464	19
d-1	0.0120	10	0.00039	2	1.46720	1.88674	5	0.282839	32	0.282835	12.7	1.1	0.61	492	10
d-4	0.0087	7	0.00030	2	1.46728	1.88673	5	0.282818	27	0.282816	11.7	0.9	0.66	474	13
d-5	0.0065	5	0.00021	1	1.46730	1.88665	6	0.282849	27	0.282847	12.9	0.9	0.59	482	13
d-20	0.0104	9	0.00035	2	1.46724	1.88630	5	0.282871	40	0.282867	13.8	1.4	0.55	488	10

$^{176}Yb/^{177}Hf = (^{176}Yb/^{173}Yb)true \times ^{173}Yb/^{177}Hf)meas \times (M173(Yb)/M177(Hf))^{\varepsilon(Hf)}$. The $^{176}LU/^{177}HF$ were calculated in a similar way by using the $^{175}Lu/^{177}Hf$. Quoted uncertainties (absolute) relate to the last quoted figure. The effect of the inter-element fractionation on the Lu/Hf was estimated to be about 6 % or less based on analyses of the GJ-1 and Plesovice zircons.

†Mean Hf signal in volt.

‡Uncertainties are quadratic additions of the within-run error and the daily reproducibility of the 40ppb-JMC475 solution. Uncertainties for the GJ-1 are 2SD.

§Initial $^{176}Hf/^{177}Hf$ and εHf calculated using the age determined by LA-ICP-MS dating (see last two rows).

¶Two-stage model age in billion years using the measured $^{176}Lu/^{177}Lu$ of each spot (first stage = age of zircon), a value of 0.0113 for the average continental crust (second stage), and a depleted mantle $^{176}Lu/^{177}Lu$ and $^{176}Hf/^{177}Hf$ of 0.0384 and 0.28325, respectively (see Gerdes and Zeh, 2006 for details and references).

**LA-ICP-MS age and error (see Table 1 for more details).

Seventy five per cent of the acquired U-Pb analyses are concordant to subconcordant (90–105%). The result of projecting their $^{206}Pb/^{238}U$ and $^{207}Pb/^{235}U$ ratios into a concordia diagram (Fig. 2b) is a continuous cluster of ages ranging from 426 ± 11 to 515 ± 12 Ma (Middle Silurian to Middle Cambrian). However, when analyses corresponding to domains interpreted as 'cores' and to overgrowths or recrystallized domains are plotted separately, they constitute different groups of ages, despite their overlap to certain extent considering their errors. In this way, the 'cores' would represent an older event, giving a weighted average (n = 65) of 495 ± 2 Ma (mean square of weighted deviates (MSWD) = 2), whereas the overgrowths would represent a younger event, for which the weighted average (n = 32) gives 475 ± 2 Ma (MSWD = 2). It could be argued that the analyses do not represent two different events, but instead their spreading would result from analytical scattering or to a certain degree of Pb loss. However, the Lu-Yb-Hf isotope data, which will be stated below, support the existence of these two separate although temporarily close events. In addition, the overgrowths/recrystallized domains have lower Th/U ratios compared with the cores, which are usually common in zircons developed during a metamorphic event (Fig. 2c).

The 53 Lu-Yb-Hf analyses performed in domains considered as cores yielded a spectrum of initial $^{176}Hf/^{177}Hf$ ranging from 0.282808 to 0.282898, which, although similar to the values obtained in the 24 analyses corresponding to overgrowths or recrystallized domains (from 0.282808 to 0.282867), is somehow wider (Fig. 2d). Slightly variable initial $^{176}Hf/^{177}Hf$ ratio is a common phenomenon in magmatic zircons, and suggests that they crystallized within a short interval from the magma, which had a heterogeneous (not equilibrated) hafnium isotopic composition (Zeh *et al.*, 2009). The difference in the Hf isotopic composition between older and younger zircon domains depends on three factors: the time span between the two zircon growth events, the relative proportion of dissolved cores and newly formed overgrowths, and the Lu/Hf ratio of the rock (Gerdes and Zeh, 2009). The lapse of time between both events is too short for the radioactive ^{176}Lu present in the rock to decay generating enough radiogenic ^{176}Hf to change noticeably the $^{176}Hf/^{177}Hf$ of the newly formed zircon, and this is the reason why both cores and overgrowths have similar $^{176}Hf/^{177}Hf$. In addition, although the zircons of this sample most likely developed resorption processes, the amount of Hf released during the dissolution of old zircon does not seem to be significant enough to modify the radiogenic Hf in the rock. Anyway, a noticeable fact is the narrower range of values in the analyses corresponding to overgrowths, which is usually a consequence of isotope homogenization during high temperature metamorphism. Further and clearer evidence of the occurrence of two separate events is registered in the variation in $^{176}Lu/^{177}Hf$, and especially in $^{176}Yb/^{177}Hf$ ratios, which are lower in the overgrowths/recrystallized domains (Fig. 2e). Certain metamorphic mineral phases such as orthopyroxene and garnet have strong affinity for heavy rare earth elements (Yb, Lu) and consequently, the zircon coeval with these minerals will be depleted in these elements compared with the magmatic zircon (Gerdes and Zeh, 2009; Abati *et al.*, 2010). Although the amphibolite sample here studied does not preserve any of these metamorphic minerals, they have been observed in the granulites, which are still preserved forming part of the ophiolite.

Initial εHf values corresponding to the analysed zircons vary from 11.6 to 15.5 in the cores, and from 11.2 to 13.8 in the overgrowths/recrystallized domains. All of them lay within the range corresponding to the depleted mantle at the age of 450–500 Ma (Fig. 2f; Chauvel and Blichert-Toft, 2001; Vervoort and Blichert-Toft, 1999). These juvenile values suggest that the gabbros constituting the Bazar ophiolite derive from a source with an isotope signature similar to that of the depleted mantle, and there was no crustal or older component involved in their generation. This is compatible with the features observed in the whole rock geochemistry of these amphibolites mentioned before, and in this way, their εHf signature also supports the hypothesis, which explains their tectonic setting in connection with a mid-ocean ridge.

Discussion

The low-to-intermediate-P granulite-facies metamorphism that affected the Bazar Ophiolite differs from the Cambrian metamorphism described in the peri-Gondwanan arc, which, in its lowest structural levels directly above the ophiolite, reached c. 10 Kb (Abati *et al.*, 2003). Moreover, the metamorphic event affecting the Bazar Ophiolite is clearly younger than the metamorphism described so far in the arc-derived terrane (c. 475 Ma vs. 496–482 Ma, respectively). On the basis of these facts and also considering the N-MORB composition of the most common mafic rocks in the ophiolite, it is clear that large sections of an oceanic lithosphere developed in a divergent plate margin were accreted, in Early Ordovician times, under a dissected peri-Gondwanan magmatic arc. The most external continental margin can be considered the most probable tectonic setting for the building of the arc (Fuenlabrada *et al.*, 2010). During a long period before the underthrusting of the ophiolitic layers, the arc experienced intra-arc accretion with development of intermediate-P granulite facies metamorphism and a subsequently important uplift and exhumation of its metamorphic belts. The regional foliation present in large regions of the uppermost units of the Órdenes Complex has Cambrian age and it is preserved relatively intact and with little Variscan reworking (Abati *et al.*, 1999, 2007; Díaz García *et al.*, 2010). The origin of the granulitic metamorphism affecting the accreted ophiolite is not clear, but it could be explained both by overheating associated with the lowest levels of the arc and by the subduction of a section of the oceanic ridge and the opening of an asthenospheric window.

The Rheic Ocean opened in the Early Ordovician times with the separation of Avalonia and other arc terranes from the continental margin of Gondwana (Murphy *et al.*, 2010; Nance *et al.*, 2010). The accretionary history of the Bazar Ophiolite is not compatible with a context of a fast-spreading ocean, as it seems to have been the Rheic, whose plate velocity

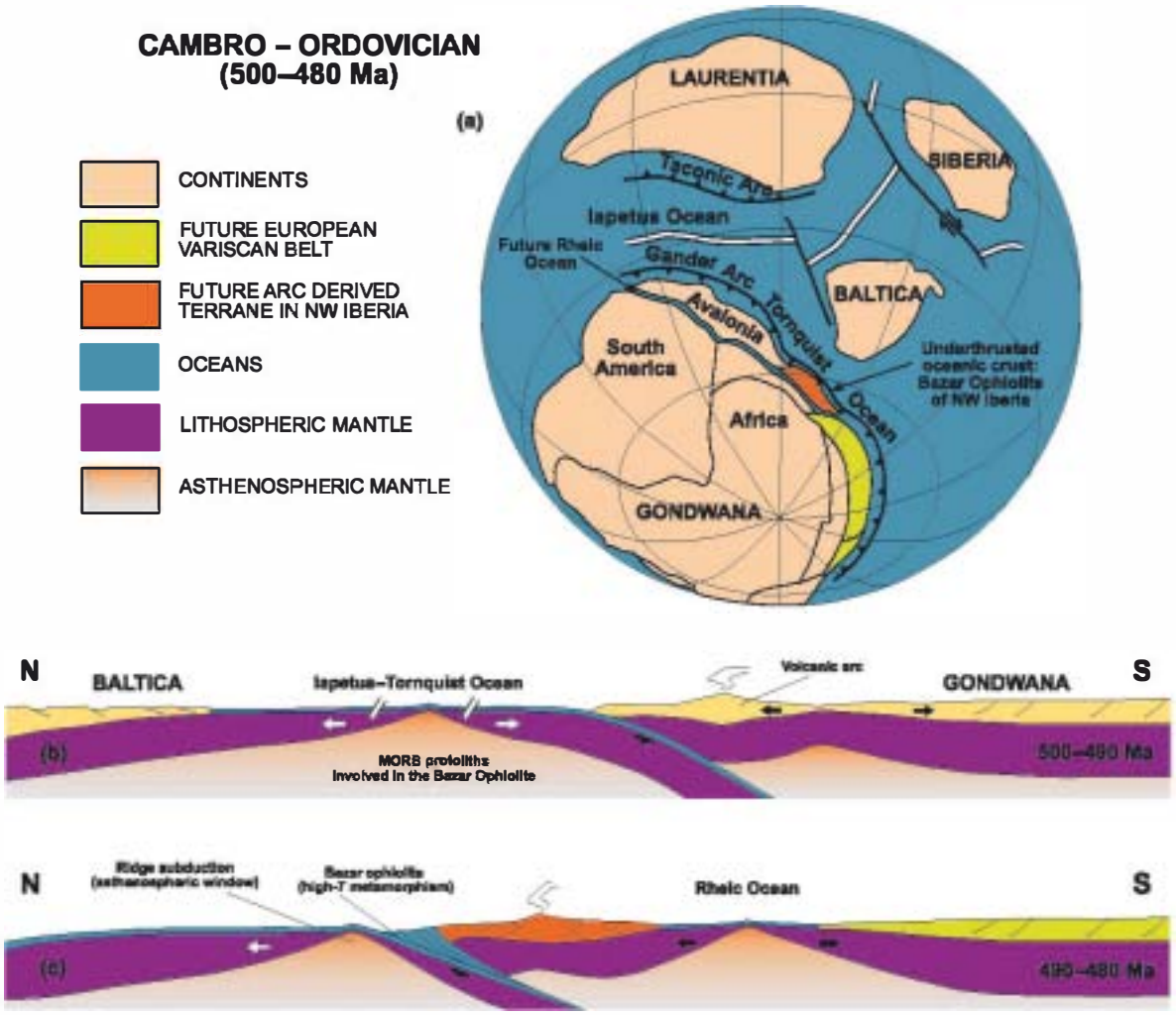

Fig. 3 Cartoon showing a palaeogeographical reconstruction and two plate sections around the Cambrian–Ordovician boundary. Largely based on Winchester *et al.* (2002), Arenas *et al.* (2007), Gómez Barreiro *et al.* (2007) and Martínez Catalán *et al.* (2009). A large magmatic arc system was a prominent feature along the continental margin of Gondwana, later rifted generating several peri-Gondwanan terranes as Avalonia and the dissected arc represented by the upper units of NW Iberia. Underthrusting of the Iapetus–Tornquist oceanic crust to the arc system allows preservation of ophiolitic units generated within the realm of this large ocean, as it is the case of the Bazar Ophiolite. The rifting of Avalonian and other minor terranes and the spreading of back-arc basins caused the opening of the Palaeozoic Rheic Ocean. This ocean was progressively wider as the peri-Gondwanan terranes drifted to the North.

has been estimated in 8–10 cm yr^{-1} (Nance *et al.*, 2010). Therefore, the generation of the oceanic crust represented in the Bazar Ophiolite was not possible within the realm of the Rheic Ocean, and may be better considered as a remnant of the Cambrian peri-Gondwanan ocean (protolith age of the mafic rocks = 495 ± 2 Ma), the Iapetus–Tornquist ocean (Fig. 3). The accretion of the ophiolite occurred during the activity of a subduction zone dipping towards Gondwana, but specific details of this accretion in relation to the opening of the Rheic Ocean are unclear. In this way, the oceanic crust could have been accreted under the arc system before the inception of the opening of the Rheic Ocean, but it could also have been underthrusted to the leading edge of a section of the arc previously rifted from the continent, during the contemporary opening of a back-arc basin. The subsequent spreading of this back-arc led to the existence of the Rheic Ocean. In any case, the Bazar Ophiolite represents an original terrane in the context of the Variscan Belt, the only relic of the peri-Gondwanan ocean previous to the opening of the Rheic described so far.

Acknowledgements

S. Sánchez Martínez thanks the Spanish Ministerio de Ciencia e Innovación, which provided her with a two-year post-doctoral contract to Goethe Universität Frankfurt am Main. Thanks also to Prof. Gerhard Brey for kindly hosting and welcoming S. Sánchez Martínez to the Department of Mineralogy and Petrology. M. Ballèvre, U. Linnemann and an anonymous referee are gratefully acknowledged for insightful reviews of the paper. Financial support for

this research has been provided by Spanish project CGL2007-65338-C02-01/BTE (Ministerio de Ciencia e Innovación).

References

Abati, J., Dunning, G.R., Arenas, R., Díaz García, F., González Cuadra, P., Martínez Catalán, J.R. and Andonaegui, P., 1999. Early Ordovician orogenic event in Galicia (NW Spain): evidence from U-Pb ages in the uppermost unit of the Órdenes Complex. *Earth Planet. Sci. Lett.*, **165**, 213–228.

Abati, J., Arenas, R., Martínez Catalán, J.R. and Díaz García, F., 2003. Anticlockwise P–T path of granulites from the Monte Castelo Gabbro (Órdenes Complex, NW Spain). *J. Petrol.*, **44**, 305–327.

Abati, J., Castiñeiras, P., Arenas, R., Fernández-Suárez, J., Gómez Barreiro, J. and Wooden, J.L., 2007. Using SHRIMP zircon dating to unravel tectonothermal events in arc environments. The early Palaeozoic arc of NW Iberia revisited. *Terra Nova*, **19**, 432–439.

Abati, J., Gerdes, A., Fernández-Suárez, J., Arenas, R., Whitehouse, M.J. and Díez Fernández, R., 2010. Magmatism and early – Variscan continental subduction in the northern Gondwana margin recorded in zircons from the basal units of Galicia, NW Spain. *Geol. Soc. Am. Bull.*, **122**, 219–235.

Arenas, R., Rubio Pascual, F.J., Díaz García, F. and Martínez Catalán, J.R., 1995. High-pressure microinclusions and development of an inverted metamorphic gradient in the Santiago Schists (Órdenes Complex, NW Iberian Massif, Spain): evidence of subduction and syn-collisional decompression. *J. Metamorph. Geol.*, **13**, 141–164.

Arenas, R., Martínez Catalán, J.R., Sánchez Martínez, S., Fernández-Suárez, J., Andonaegui, P., Pearce, J.A. and Corfu, F., 2007. The Vila de Cruces Ophiolite: a remnant of the early Rheic Ocean in the Variscan suture of Galicia (Northwest Iberian Massif). *J. Geol.*, **115**, 129–148.

Chauvel, C. and Blichert-Toft, J., 2001. A hafnium isotope and trace element perspective on melting of the depleted mantle. *Earth Planet. Sci. Lett.*, **190**, 137–151.

Corfu, F., Hanchar, J.M., Hoskin, P.W.O. and Kinny, P., 2003. Atlas of zircon textures. In: *Zircon* (J.M. Hanchar and P.W.O. Hoskin, eds), *Mineralogical Society of America, Reviews in Mineralogy and Geochemistry*, **53**, 469–500.

Díaz García, F., 1990. La geología del sector occidental del Complejo de Órdenes (Cordillera Hercínica, NW de España). *Nova Terra*, **3**, 230.

Díaz García, F., Arenas, R., Martínez Catalán, J.R., González del Tánago, J. and Dunning, G.R., 1999. Tectonic evolution of the Careón Ophiolite (northwest Spain): a remnant of oceanic lithosphere in the Variscan Belt. *J. Geol.*, **107**, 587–605.

Díaz García, F., Sánchez Martínez, S., Castiñeiras, P., Fuenlabrada, J.M. and Arenas, R., 2010. A peri-Gondwanan arc in NW Iberia. II: assessment of the intra-arc tectonothermal evolution through U-Pb SHRIMP dating of mafic dykes. *Gondwana Res.*, **17**, 352–362.

Fernández-Suárez, J., Arenas, R., Abati, J., Martínez Catalán, J.R., Whitehouse, M.J. and Jeffries, T.E., 2007. U-Pb chronometry of polymetamorphic high-pressure granulites: An example from the allochthonous terranes of the NW Iberian Variscan belt. In: *4-D Framework of Continental Crust* (R.D. Hatcher Jr, M.P. Carlson, J.H. McBride and J.R. Martínez Catalán, eds), *Geol. Soc. Am. Mem.*, **200**, 469–488.

Fuenlabrada, J.M., Arenas, R., Sánchez Martínez, S., Díaz García, F. and Castiñeiras, P., 2010. A peri-Gondwanan arc in NW Iberia. I: isotopic and geochemical constraints on the origin of the arc – a sedimentary approach. *Gondwana Res.*, **17**, 338–351.

Gerdes, A. and Zeh, A., 2006. Combined U-Pb and Hf isotope LA-(MC)ICP-MS analyses of detrital zircons: comparison with SHRIMP and new constraints for the provenance and age of an Armorican metasediment in Central Germany. *Earth Planet. Sci. Lett.*, **249**, 47–61.

Gerdes, A. and Zeh, A., 2009. Zircon formation versus zircon alteration – New insights from combined U-Pb and Lu-Hf in-situ LA-ICP-MS analyses, and consequences for the interpretation of Archean zircon from the Central Zone of the Limpopo Belt. *Chem. Geol.*, **261**, 230–243.

Gómez Barreiro, J., Martínez Catalán, J.R., Arenas, R., Castiñeiras, P., Abati, J., Díaz García, F. and Wijbrans, J.R., 2007. Tectonic evolution of the upper allochthon of the Órdenes complex (northwestern Iberian Massif): Structural constraints to a polyorogenic peri-Gondwanan terrane. In: *The evolution of the Rheic Ocean: From Avalonian – Cadomian active margin to Alleghenian – Variscan collision* (U. Linneman, R.D. Nance, P. Kraft and G. Zulauf, eds), *Geol. Soc. Am. Spec. Pap.*, **423**, 315–332.

Hoskin, P.W.O. and Black, L.P., 2000. Metamorphic zircon formation by solid – state recrystallization of protolith igneous zircon. *J. Metamorph. Geol.*, **28**, 423–439.

Martínez Catalán, J.R., Arenas, R., Díaz García, F., Rubio Pascual, F.J., Abati, J. and Marquínez, J., 1996. Variscan exhumation of a subducted Paleozoic continental margin: the basal units of the Órdenes Complex, Galicia, NW Spain. *Tectonics*, **15**, 106–121.

Martínez Catalán, J.R., Arenas, R., Abati, J., Sánchez Martínez, S., Díaz García, F., Fernández Suárez, J., González Cuadra, P., Castiñeiras, P., Gómez Barreiro, J., Díez Montes, A., González Clavijo, E., Rubio Pascual, F.J., Andonaegui, P., Jeffries, T.E., Alcock, J.E., Díez Fernández, R. and López Carmona, A., 2009. A rootless suture and the loss of the roots of a mountain chain: the Variscan belt of NW Iberia. *C.R. Geoscience*, **341**, 114–126.

Matte, P., 2001. The Variscan collage and orogeny (480–290 Ma) and the tectonic definition of the Armorica microplate: a review. *Terra Nova*, **13**, 122–128.

Murphy, J.B., Keppie, J.D., Nance, D. and Dostal, J., 2010. Comparative evolution of the Iapetus and Rheic Oceans: Aa North America perspective. *Gondwana Res.*, **17**, 482–499.

Nance, D., Gutiérrez-Alonso, G., Keppie, J.D., Linnemann, U., Murphy, J.B., Quesada, C., Strachan, R.A. and Woodcock, N.H., 2010. Evolution of the Rheic Ocean. *Gondwana Res.*, **17**, 194–222.

Ordoñez Casado, B., Gebauer, D., Schäfer, H.J., Gil Ibarguchi, J.I. and Peucat, J.J., 2001. A single Devonian subduction event for the HP/HT metamorphism of the Cabo Ortegal complex within the Iberian Massif. *Tectonophysics*, **332**, 359–385.

Pearce, J.A., 1996. A users guide to basalt discrimination diagrams. In: *Trace Element Geochemistry of Volcanic Rocks: Application for Massive Sulphide Exploration* (D.A. Wyman, ed), *Short Course Notes, Geological Association of Canada*, **12**, 79–113.

Sánchez Martínez, S., 2009. Geoquímica y Geocronología de las ofiolitas de Galicia. *Nova Terra*, **37**, 351.

Sánchez Martínez, S., Arenas, R., Díaz García, F., Martínez Catalán, J.R., Gómez Barreiro, J. and Pearce, J., 2007. The Careón Ophiolite, NW Spain: supra-subduction zone setting for the youngest Rheic Ocean floor. *Geology*, **5**, 53–56.

Sánchez Martínez, S., Arenas, R., Fernández-Suárez, J. and Jeffries, T.E., 2009. From Rodinia to Pangaea: ophiolites from NW Iberia as witness for a long-lived continental margin. In: *Ancient Orogens and Modern Analogues* (J.B. Murphy, J.D. Keppie and A.J. Hynes, eds), *Geological Society, London, Special Publications*, **327**, 317–341.

Vervoort, J.D. and Blichert-Toft, J., 1999. Evolution of the depleted mantle: Hf isotope evidence from juvenile rocks through time. *Geochim. Cosmochim. Acta*, **63**, 533–556.

Winchester, J.A., Pharaoh, T.C. and Verniers, J., 2002. Palaeozoic amalgamation of Central Europe: an introduction and synthesis of new results from recent geological and geophysical investigations. In: *Palaeozoic Amalgamation of Central Europe* (J.A. Winchester, T.C. Pharaoh and J. Verniers, eds), *Geological Society, London, Special Publications*, **201**, 1–18.

Wood, D.A., 1980. The application of a Th-Hf-Ta diagram to problems of tectomagmatic classification and to establishing the nature of crustal contamination of basaltic lavas of the British Tertiary Volcanic Province. *Earth Planet. Sci. Lett.*, **50**, 11–30.

Zeh, A., Gerdes, A. and Barton J.M. Jr, , 2009. Archean accretion and crustal evolution of the Kalahari Craton – The zircon age and Hf isotope record of granitic rocks from Barberton/Swaziland to the Francistown Arc. *J. Petrol.*, **50**, 933–966.